Journal of Alloys and Compounds 508 (2010) 494–499

Contents lists available at ScienceDirect

Journal of Alloys and Compounds

journal homepage: www.elsevier.com/locate/jallcom

Influence of Fe_2O_3 doping on microstructural and electrical properties of ZnO–Pr_6O_{11} based varistor ceramic materials

Zhijian Peng[a,*], Xiuli Fu[b], Yanxu Zang[a], Zhiqiang Fu[a], Chengbiao Wang[a], Longhao Qi[c], Hezhuo Miao[c]

[a] School of Engineering and Technology, China University of Geosciences, Beijing 100083, PR China
[b] Faculty of Science, Beijing University of Posts and Telecommunications, Beijing 100876, PR China
[c] State Key Lab of New Ceramics and Fine Processing, Tsinghua University, Beijing 100084, PR China

ARTICLE INFO

Article history:
Received 9 March 2010
Received in revised form 17 August 2010
Accepted 24 August 2010
Available online 22 September 2010

PACS:
84.32.Ff
61.72.−y

Keywords:
ZnO varistor
Pr_6O_{11}
Fe_2O_3
Doping
Electrical properties

ABSTRACT

The doping effect of Fe_2O_3 on the microstructural and electrical properties of ZnO–Pr_6O_{11} based varistor ceramic materials was investigated. Fe_2O_3 doping would inhibit the growth of ZnO grains, whose average sizes were found to decrease from 3.0 to 2.7 μm with the doping level of Fe_2O_3 increased from 0 to 1 mol%. When the doping level of Fe_2O_3 was 0.005 mol%, the varistors exhibited the optimum nonlinear electrical characteristics with nonlinear coefficient of about 26, breakdown voltage of approximately 571 V/mm and leakage current of less than 65 μA. With higher doping level of Fe_2O_3, more Fe atoms would segregate at grain boundaries, providing more extra electrical carriers, decreasing the resistances of the grain boundaries, and $PrFeO_3$ would be formed, destroying the construction of grain boundaries. Therefore, the nonlinear electrical properties of the resultant varistor materials were deteriorated.

1. Introduction

ZnO-based varistors are polycrystalline electronic ceramic devices, which are obtained by sintering ZnO powder with small amounts of other metal oxides. The most excellent property of ZnO varistor materials is their nonlinear voltage–current characteristics due to the potential barriers formed at grain boundaries. Their primary function is to protect electronics and electrical circuits from being destroyed by transient voltage surges, and this protection function can be performed promptly and repeatedly. So they are very much useful both in power industry as well as in electronic industry [1–5].

The conducting mechanism of ZnO-based varistors is a double Schottky phenomenon. The key that a ZnO-based varistor functions is the formation of grain boundary layer of high electrical resistivity. According to the different varistor forming oxides in the grain boundary layer, ZnO-based varistor materials are classified into Bi-doped, Pr-doped, V-doped and Ca-doped ZnO varistor materials, and so on [5,6]. Other oxides are doped into varistor ceramics to achieve, hopefully, a larger nonlinear coefficient and higher resistivity [7–12].

Up to now, the majority of commercial ZnO varistor materials are Bi-doped ZnO-based semiconductors [5,6]. However, the most commercially applied Bi-doped ZnO varistor materials have a few drawbacks due to the high volatility and reactivity of Bi_2O_3 during liquid sintering. The former changes varistor characteristics with the deviation of inter-composition ratio of additives, and the latter destroys the multi-layer structure of chip varistors, which generates an insulating spinel phase deteriorating surge-absorption capabilities [5,13,14]. To overcome these problems, various fabrication techniques to reduce the volatility have been continuously developed for Bi-doped ZnO varistor materials [2,13–18], and different varistor forming oxides have been tentatively investigated into ZnO varistor materials [19–24], in which Pr-doped ZnO varistor materials are most promising in application and have been intensively studied [19–22], due to their advantages over Bi-doped ZnO varistor materials in relatively simple two-phase microstructure of ZnO grains and praseodymium oxide intergranular phases, reducing quantity of composition materials and improving the electrical properties of the ceramics, and stable composition at high temperature sintering stemming from the high melting point of Pr_6O_{11} [5,21].

* Corresponding author. Tel.: +86 10 82320255; fax: +86 10 82322624.
E-mail address: pengzhijian@cugb.edu.cn (Z. Peng).

0925-8388/$ – see front matter © 2010 Elsevier B.V. All rights reserved.
doi:10.1016/j.jallcom.2010.08.100

It is a pity, however, that Pr-doped ZnO varistor materials have not been studied as extensively as done for the Bi-doped ZnO varistor materials. As main dopants, to our knowledge, only the effects of Co-doping and rare-earth doping on the microstructural and electrical properties of Pr-doped ZnO varistor materials have been reported in literature. And several other kinds of metal oxides such as MnO_2, Sb_2O_3, Al_2O_3, NiO, Cr_2O_3, TiO_2 and K_2O which are commonly used in the ZnO–Bi_2O_3 system were tried into Pr-doped ZnO varistor materials [5,19–22]. Their mutual interactions, especially the one between the varistor forming oxide, Pr_6O_{11}, and other electrical property improvers, have been under dimness.

For example, it was reported that Fe_2O_3 would be a fatal additive for ZnO–Bi_2O_3 system [25], but Song and Liu [26] claimed that when the content of Fe_2O_3 was less than 0.1 mol% in ZnO–Bi_2O_3 system, it could improve the electrical properties of ZnO–Bi_2O_3 based varistor materials. However, the influence of Fe_2O_3 doping on ZnO–Pr_6O_{11} based varistor materials has not been reported. So, the aim of this work is to investigate the effect of Fe_2O_3 doping (which is hardly to be avoided during the industrial production of ZnO varistors due to the usage of iron-made equipments) on the microstructural and electrical properties of ZnO–Pr_6O_{11} based varistor materials, and to try to understand the mutual interaction and reaction mechanism between the oxides in the material system.

2. Experimental procedures

2.1. Sample preparation

The samples were fabricated using a conventional ceramic process [27,28] with a nominal composition of $(98.0-x)$mol% ZnO + 0.5 mol% Pr_6O_{11} + 1.0 mol% Co_3O_4 + 0.5 mol% Cr_2O_3 + $x$mol% Fe_2O_3 (x = 0.0, 0.001, 0.003, 0.005, 0.01, 0.025, 0.1, 0.5, 1.0). The powder mixtures were ball-milled in water for 24 h with highly wear-resistant ZrO_2 as media, in which the weight ratio of ZrO_2 balls to powder mixture was 2:1. The milled slurries were dried in air at 120 °C for at least 24 h. The dried powder mixtures were then crashed into fine powders, sieved, and pressed into discs of 6.0 mm in diameter and 2.0 mm in thickness. The prepared green bodies have a density between 2.8 and 3.5 g/cm^3. And then the green discs were sintered at 1300 °C in air for 1 h with heating rates of 2 °C/min and cooling naturally. To measure the electrical properties, silver pastes were coated and toasted on both sides of the sintered samples.

2.2. Materials characterization

The sample densities were measured by Archimedes method according to international standard (ISO18754). The phase compositions of the sintered samples were identified by X-ray diffractometer (XRD, D/max2550HB+/PC, Cu Kα and λ = 1.5418 Å) through a continuous scanning mode with speed of 8°/min. The fractural surfaces of the as-prepared samples were observed via SSX-550 scanning electron microscope (SEM), and the polished surfaces of the samples were examined using LEO-1530 scanning electron microscope equipped with energy dispersive X-ray spectroscopy (EDX). The average sizes (d) of ZnO grains were determined using linear intercept method from the SEM images of the polished samples.

The electric field to current density (E–J) characteristics of the as-prepared samples was measured at room temperature with a high-voltage source measurement unit (Model: CJ1001). The varistor voltage (V_B) was determined at 1 mA/cm^2 (V_{1mA}) and the nonlinear coefficient (α) was calculated using

$$\alpha = \frac{\log(J_2/J_1)}{\log(E_2/E_1)} = \frac{1}{\log(E_2/E_1)} \quad (1)$$

where E_1 and E_2 are the voltage fields corresponding to J_1 = 1 mA/cm^2 and J_2 = 10 mA/cm^2, respectively. The leakage current (I_L) was determined at 0.75 V_{1mA}.

The applied voltage per grain boundary (V_{gb}) was calculated using

$$V_{gb} = V_B \frac{d}{D} \quad (2)$$

where V_B is the varistor voltage of the ceramic varistors, d is the average size of ZnO grains, and D is the thickness of the sintered samples.

The dependence of impedance (reactance Z'' and resistance Z') of the ceramic varistors on frequency was determined with an Agilent 4294A impedance analyzer in the frequency range of 40 Hz–15 MHz at temperature of 250 °C.

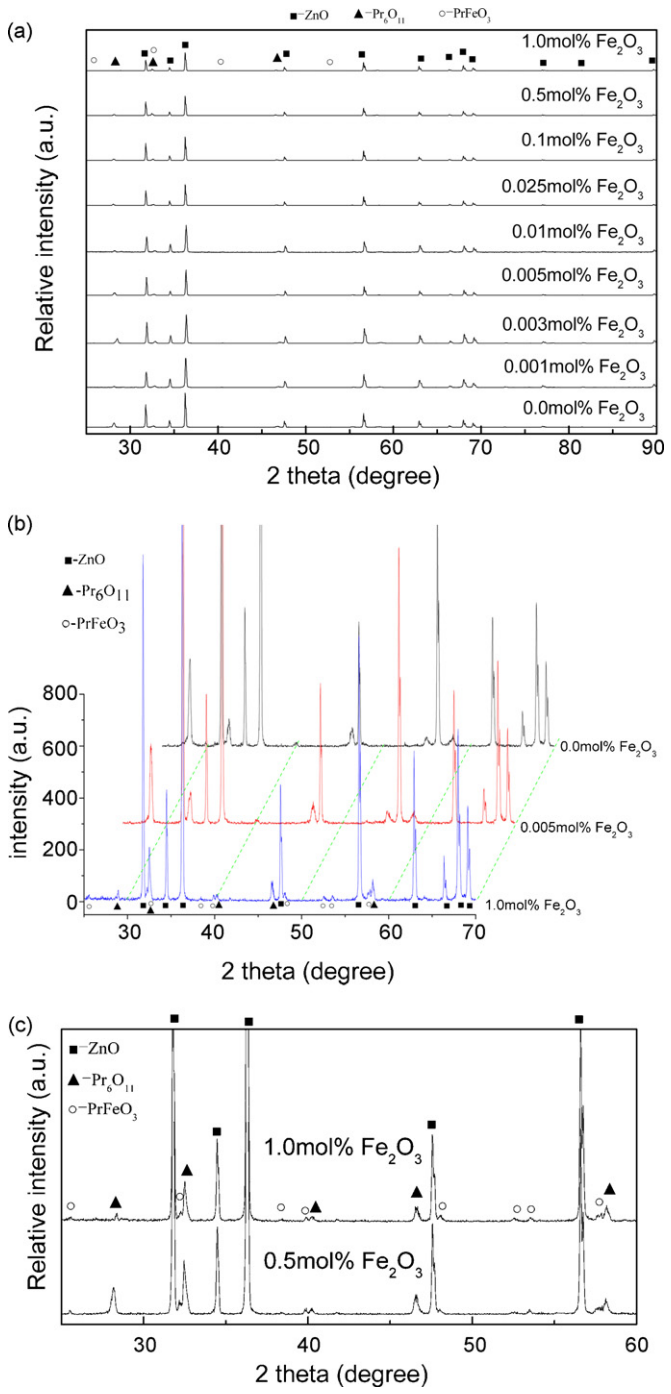

Fig. 1. XRD patterns of typical samples doped with different amounts of Fe_2O_3 (a), in which the samples doped with 0.0 mol%, 0.05 mol% and 1.0 mol% Fe_2O_3 were magnified in (b), and the samples doped with 0.5 mol% and 1.0 mol% Fe_2O_3 were compared in (c).

3. Results and discussion

3.1. Composition and microstructure

Fig. 1a shows the XRD patterns with normalized peak intensities of the as-prepared ZnO–Pr_6O_{11} based varistor ceramic samples doped with different amounts of Fe_2O_3. The experimental results indicate that, when the doping amounts of Fe_2O_3 into the samples are less than 0.10 mol%, the identifiable phases in the samples are almost the same as that in the sample without Fe_2O_3 doped, where excepting the major phase of ZnO, only could praseodymium

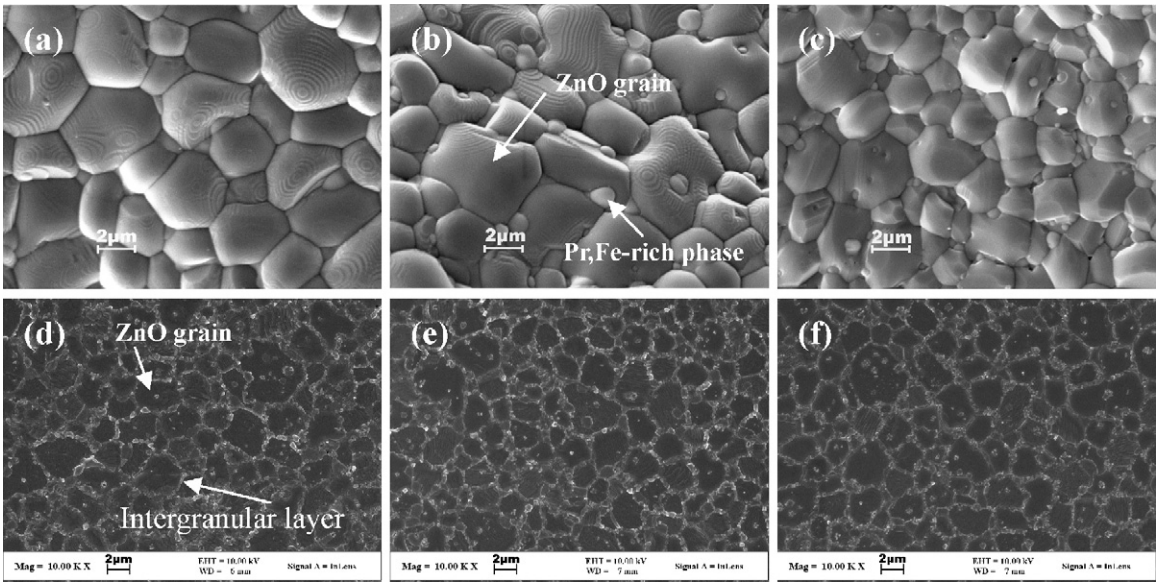

Fig. 2. SEM micrographs of typical samples doped with different amounts of Fe_2O_3: (a) fractural surface without Fe_2O_3; (b) fractural surface with 0.005 mol% Fe_2O_3; (c) fractural surface with 1.0 mol% Fe_2O_3; (d) polished surface without Fe_2O_3; (e) polished surface with 0.005 mol% Fe_2O_3 and (f) polished surface with 1.0 mol% Fe_2O_3.

oxide (Pr_6O_{11}) be detected, as can be seen in Fig. 1a and b. But when the doping amount of Fe_2O_3 was increased up to 0.5 mol%, the third phase, $PrFeO_3$, was detected, as can be clearly observed in the magnified pattern shown in Fig. 1b and c. And Fig. 1c also indicates that, with the increase in doping amounts of Fe_2O_3, the relative intensities of the diffraction peaks of Pr_6O_{11} phase declined, but the relative intensities of the diffraction peaks of $PrFeO_3$ phase enhanced. This phenomenon could be attributed to the reaction of Fe_2O_3 with Pr_6O_{11} during sintering, which would produce $PrFeO_3$. And as can be seen in the figure, the more Fe_2O_3 was added, the more $PrFeO_3$ would be produced.

Fig. 2 illustrates the SEM micrographs of typical ZnO–Pr_6O_{11} based varistor ceramic samples doped with different amounts of Fe_2O_3, in which Fig. 2a–c was taken from the fractural surfaces of the samples and Fig. 2d–f was from the polished surfaces of the corresponding samples as illustrated in Fig. 2a–c. From Fig. 2a–f, it can be seen that there is nearly no porosity in the sintered samples, indicating that the samples are almost fully dense, which is consistent with the quiet high relative density of the as-prepared samples listed in Table 1. And Fig. 2d–f reveals that the microstructures of Fe_2O_3-doped samples are similar to that of Fe_2O_3-undoped sample, probably implying that the doping of Fe_2O_3 would not change the crystalline structure of the as-prepared ZnO varistor ceramic materials, but the levels of electrical carriers. Moreover, from Fig. 2d–f, one can also see that the microstructures of the varistor ceramics primarily consist of ZnO grain (main phase) and white continuous intergranular phase (second phase), which can also be confirmed by Fig. 3.

Fig. 3 reveals the corresponding EDX analysis results of typical Fe_2O_3-doped ZnO–Pr_6O_{11} based varistor ceramic samples. It was found that the grain phase mainly consisted of Zn and O atoms, and tricky amount of Pr, Fe, Co and Cr atoms; on the other hand, the continuous intergranular phase mainly composed of Pr, Fe and O atoms, indicating that Pr and Fe elements were mainly distributed at the gain boundaries. The reason for this phenomenon is possibly attributed that the ionic radius of Pr^{3+} (0.1013 nm) is much bigger than that of Zn^{2+} ion (0.0740 nm), and thus the solubility of Pr ions into the ZnO grain is limited [29,30]. Combined with the results of the XRD analysis shown in Fig. 1, it could be concluded that the grain was ZnO phase but with tricky amount of Fe-, Co-, Cr- and Pr-doped, and the continuous intergranular phase was a mixture of praseodymium oxides and $PrFeO_3$ (Pr- and Fe-rich phase but with small amounts of Co and Cr merged in).

It should be noted from the EDX results that the doped Fe atoms existed both in ZnO grains and at the grain boundaries. With the doping levels of Fe_2O_3 increased, the contents of Fe atoms both in ZnO grains and at the grain boundaries increased. The reason for this phenomenon is that the radius of Fe^{3+} ions (0.0645 nm) is smaller than that of Zn^{2+} ions (0.0740 nm) [30,31]. So, the Fe^{3+} ions added in could dissolve into ZnO grains during sintering, and the more Fe_2O_3 was doped, the more Fe^{3+} ions dissolved into the ZnO grains.

However, it is impossible that all the doped Fe atoms would dissolve into ZnO grains because of the compositional balance of Fe atoms between ZnO crystalline phase and the second phase, and the saturation of Fe^{3+} doped in ZnO crystalline phase due to the different crystal structures of Fe_2O_3 and ZnO. So, a small portion of the added Fe^{3+} ions would segregate at the grain boundaries [32] when the doping level is low, and most of them would segregate at the grain boundaries when the doping level is high.

And moreover, the added Fe^{3+} ions segregating at the grain boundaries would, in fact, react with praseodymium oxide, producing $PrFeO_3$, which is a phase of perovskite structure [33,34] and identified by XRD as shown in Fig. 1. The resultant $PrFeO_3$ phase segregating at the grain boundaries pins at the grain boundaries of ZnO, playing a role of inhibitor to the growth of ZnO grains. And this was confirmed by the decrease of the average size of ZnO grains from 3.0 to 2.7 μm, and the higher densification of the sintered ceramic bodies with increased density from 5.55 to 5.68 g/cm^3 and relative density from 96.7% to 99.1%, when the doping levels of Fe_2O_3 increased from 0 to 1 mol%. More detailed microstructural parameters are summarized in Table 1.

3.2. Electrical properties

Fig. 4 shows the *E–J* characteristics of the as-prepared samples doped with different amounts of Fe_2O_3. It is known that in such figure, the sharper the knee of the curves between the linear region and the breakdown field, the better the nonlinear characteristics. In this case, when the doping levels of Fe_2O_3 are no more than 0.005 mol%, with more Fe_2O_3 doped, the knees become more pronounced, so the nonlinear properties of the varistor ceramic

Table 1
Microstructural and *E–J* characteristic parameters of ZnO–Pr_6O_{11} based varistor ceramic samples doped with different amounts of Fe_2O_3.

Fe_2O_3 content (mol%)	Grain size, *d* (μm)	Sample thickness, *D* (mm)	Apparent density (g/cm^3)	Theoretical density (g/cm^3)	Relative density (%)	V_B (V/mm)	α	I_L (μA)	V_{gb} (V)
0	3.0	1.76	5.55	5.74	96.7	270	12	120	0.45
0.001	3.0	1.74	5.55	5.74	96.7	308	13	117	0.52
0.003	2.9	1.77	5.56	5.74	96.9	485	17	95	0.79
0.005	2.8	1.76	5.56	5.74	96.9	571	26	65	0.90
0.01	2.9	1.75	5.58	5.74	97.2	415	19	110	0.68
0.025	2.8	1.73	5.59	5.74	97.4	339	16	180	0.56
0.1	2.7	1.74	5.63	5.74	98.1	320	12	210	0.50
0.5	2.7	1.75	5.68	5.73	99.1	129	4	415	0.20
1.0	2.7	1.77	5.66	5.71	99.1	11	2	690	0.02

Note: The theoretical density was defined on the condition that in the sintered bodies of the ceramics, all the doped Fe_2O_3 reacted with Pr_6O_{11} into $PrFeO_3$ phase, and the left phases were ZnO and Pr_6O_{11}.

materials become better. But the nonlinear properties are deteriorated with more Fe_2O_3 added when the doping levels of Fe_2O_3 are higher than 0.005 mol%. The detailed *E–J* parameters are listed in Table 1.

From Table 1, it can be seen that the nonlinear coefficient of the varistor ceramic materials would increase as the doping amounts of Fe_2O_3 increased when the doping levels of Fe_2O_3 are no more than 0.005 mol%, but the nonlinear coefficient would dramatically decrease with too much more Fe_2O_3 added. At the doping level of Fe_2O_3 0.005 mol%, the nonlinear coefficient reached at the highest value, 26.

As can be seen from the EDX analysis, some Fe^{3+} ions added could enter into the ZnO grains during sintering. Because the radius of Fe^{3+} ions (0.0645 nm) is smaller than that of Zn^{2+} ions (0.0740 nm), the introduction of Fe_2O_3 into ZnO lattice should lead to the reaction [25]

$$Fe_2O_3 \xrightarrow{ZnO} 2Fe_{Zn}^{\bullet} + 2O_o^x + 2e' + \frac{1}{2}O_2 \quad (3)$$

where the Kröger–Vink symbols were used. So, it can be seen that, in ZnO varistor ceramics, Fe^{3+} acts as a donor, providing extra electrical carriers when some Fe^{3+} ions enter into the ZnO grains. The carriers could improve the conductivity of ZnO grains, which can be easily observed from the complex impedance spectra as shown in Fig. 5. And this process is beneficial to improve the nonlinear properties of ZnO ceramic varistors, that is, to obtain varistor ceramic materials with high nonlinear coefficient. And more, the oxygen generated from the chemical-defect reaction will be partly absorbed at ZnO grain boundaries, easily capturing electrons to become negatively charged ions, contributing the formation of boundary barriers [35]. And Ref. [36] had also addressed that the absorbed oxygen at the grain boundaries would generate electronic interface states at the grain boundaries, which is also helpful for obtaining a high nonlinear property. So, to certain extent, these two processes are positive to obtain high-performance varistor ceramic materials.

However, when the doping level of Fe_2O_3 is much high, too more Fe ions would be segregated at the grain boundaries, so the density of electrical carriers at the grain boundaries would be high, and the resistance of the grain boundaries would be reduced, which can also be observed from the complex impedance spectra shown in Fig. 5, thus decreasing the barrier height. In such case, the doping of Fe_2O_3 would have negative effect on the nonlinear coefficient of the varistor ceramic materials [37].

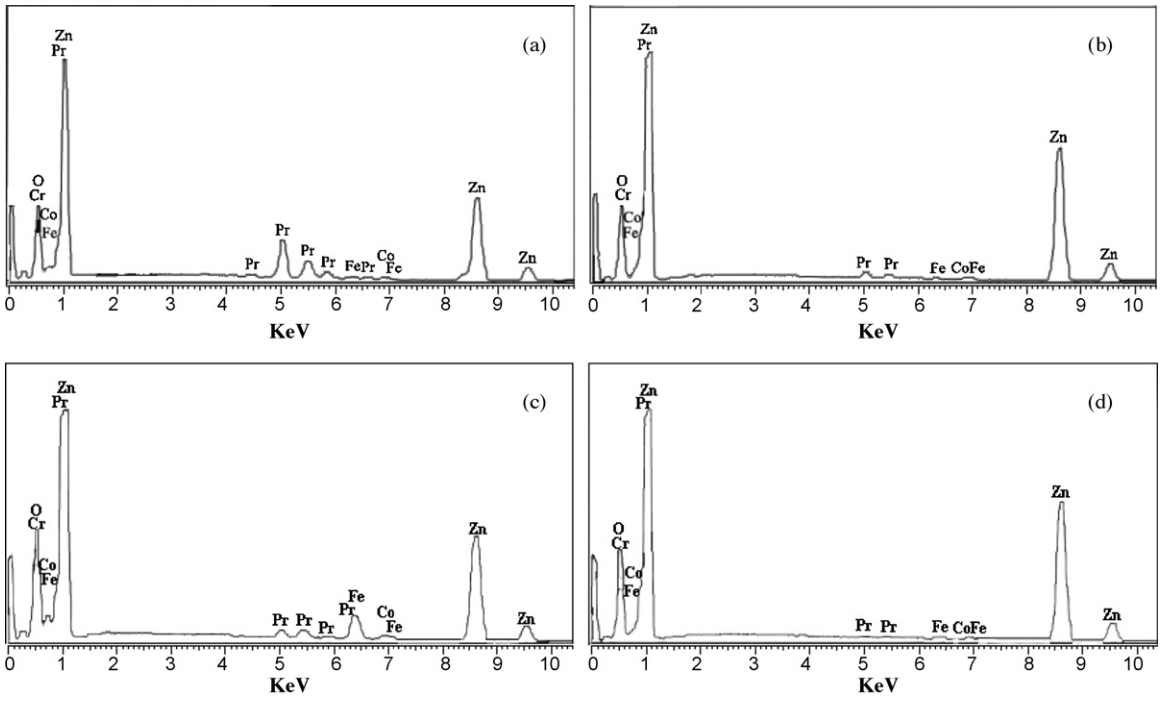

Fig. 3. The EDX spectra recorded from intergranular layer or ZnO grain of typical samples doped with different amounts of Fe_2O_3: (a) intergranular layer with 0.005 mol% Fe_2O_3; (b) ZnO grain with 0.005 mol% Fe_2O_3; (c) intergranular layer with 0.5 mol% Fe_2O_3 and (d) ZnO grain with 0.5 mol% Fe_2O_3.

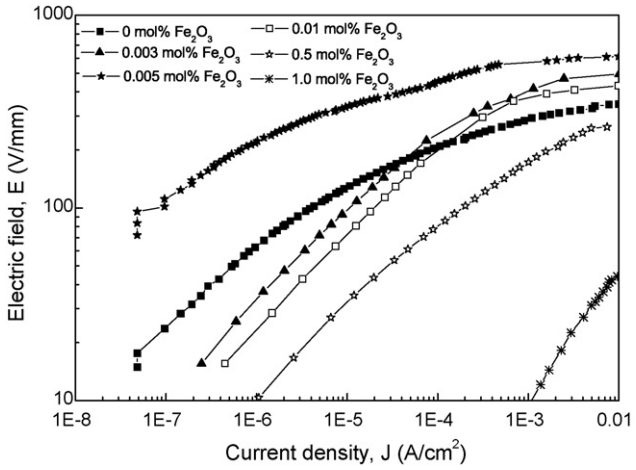

Fig. 4. *E–J* characteristics of typical samples doped with different amounts of Fe_2O_3.

Like the dependence of the nonlinear coefficient of the as-prepared varistor ceramic materials on the doping level of Fe_2O_3, their varistor voltages had the similar change tendency with the variation of the doping levels of Fe_2O_3. In this work, when the doping level of Fe_2O_3 was 0.005 mol%, the breakdown voltage had the highest value, 571 V/mm.

The varistor voltages of ZnO–Pr_6O_{11} based varistor ceramic materials have correlated to the grain size of ZnO in the samples and the applied voltage per grain boundary. The varistor voltages of the ceramic varistors are positively proportional to the number of grain boundaries between the two applied electrodes, but in inverse proportion with the ZnO grain sizes. As can be seen from Table 1, with the doping levels of Fe_2O_3 increased, the ZnO grain sizes decrease gradually but in a quite narrow range. Thus, the applied voltage per grain boundary plays a quite important role in the variation of the varistor voltages.

The applied voltage per grain boundary of the as-prepared samples is relatively low as compared with the reported value in literature [22], because high-impedance grain boundaries are not formed during the sintering. As can be seen in Fig. 2, there are too much intergranular phases formed at the ZnO grains, and the intergranular phase is Pr-rich phase as confirmed by XRD and EDX. The rare-earth metal oxide layer itself is of low electrical resistance because of its high concentration of defects [38]. In addition, as presented above, when the doping level of Fe_2O_3 is much high, too more Fe ions would be segregated at the grain boundaries, reducing the resistance of the grain boundaries. In short, these two mechanisms lead to a low-impedance grain boundary, and that is why the grain size of the samples is so small but the breakdown voltage is not high.

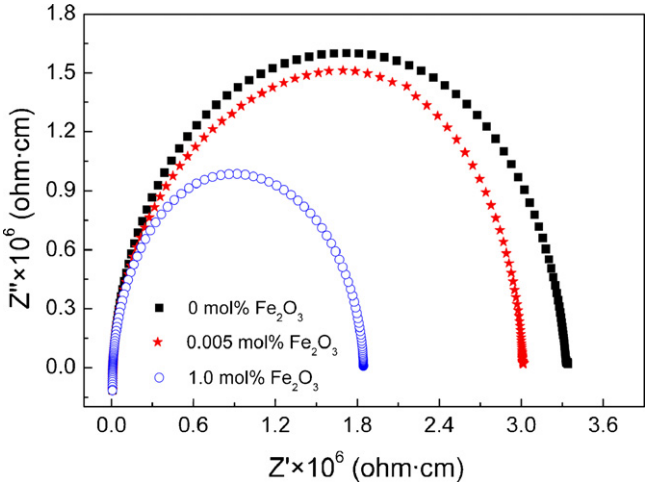

Fig. 5. Complex impedance spectra of typical samples doped with different amounts of Fe_2O_3.

Generally speaking, the variation of the leakage current of varistor ceramics is opposite to that of the nonlinear exponent, which can also be seen in Table 1. A high value of nonlinear exponent of varistor ceramics would lead to low leakage current due to its relatively high tunneling current, and a low value of nonlinear exponent would lead to high leakage current due to its relatively high thermionic emission current [39].

4. Conclusions

In ZnO–Pr_6O_{11}–Co_3O_4–Cr_2O_3–Fe_2O_3 based varistor ceramic materials, Fe_2O_3 was an important additive, acting as an inhibitor of ZnO grain growth. With tricky and appropriate amount of Fe_2O_3 doped, the electrical property of ZnO–Pr_6O_{11} based varistor ceramics would be significantly improved. When the doping level of Fe_2O_3 was no more than 0.005 mol%, more addition of Fe_2O_3 could improve the nonlinear coefficient and varistor voltage of the materials. The optimum nonlinear coefficient, 26, and varistor voltage, 571 V/mm, were acquired when the doping level of Fe_2O_3 was 0.005 mol%. Too much more of Fe_2O_3 doped would destroy the nonlinear properties of the ceramic materials.

Acknowledgments

This work was supported by "Scientific Research Foundation for Returned Overseas Chinese Scholars, State Education Ministry", the National Natural Science Foundation of China (grant no. 60806005), "Transfer and Industrialization Project of Sci-Tech Achievement, Cooperation Project between University and Factory, Beijing Municipal Commission of Education", and "State Key Laboratory of New Ceramic and Fine Processing, Tsinghua University (grant no. KF0903)".

References

[1] K.T. Gupta, J. Am. Ceram. Soc. 73 (1990) 1817–1840.
[2] D. Xu, L.Y. Shi, Z.H. Wu, Q.D. Zhong, X.X. Wu, J. Eur. Ceram. Soc. 29 (2009) 1789–1794.
[3] H. Mourad, M. Renaud, Ceram. Int. 35 (2009) 1385–1389.
[4] S. Bernik, G. Branković, S. Rustja, M. Žunić, M. Podlogar, Z. Branković, Ceram. Int. 34 (2008) 1495–1502.
[5] H. Feng, Z.J. Peng, X.L. Fu, Z.Q. Fu, C.B. Wang, L.H. Qi, H.Z. Miao, J. Alloys Compd. 497 (2010) 304–307.
[6] C.W. Nahm, Ceram. Int. 35 (2009) 2679–2685.
[7] S.A. Wan, W.Z. Lu, W. Liu, Jpn. J. Appl. Phys. 49 (2010) 061102.
[8] W.C. Long, J. Hu, J. Liu, J.L. He, Mater. Lett. 64 (2010) 1081–1084.
[9] Z.H. Wu, J.H. Fang, D. Xu, Q.D. Zhong, L.Y. Shi, Int. J. Min. Met. Mater. 17 (2010) 86–91.
[10] L.H. Cheng, L.Y. Zheng, G.R. Li, K.Y. Yuan, Y. Gu, F.P. Zhang, J. Am. Ceram. Soc. 93 (2010) 44–47.
[11] A. Pandey, A. Prasad, S. Singh, O. Parkash, D. Kumar, J. Mater. Sci. 19 (2008) 1122–1127.
[12] M. Takada, S. Yoshikado, J. Eur. Ceram. Soc. 30 (2010) 531–538.
[13] L. Ke, D.M. Jiang, C.X. Wang, X.M. Ma, Mod. Phys. Lett. B23 (2009) 3013–3022.
[14] D. Xu, X.N. Cheng, X.H. Yan, H.X. Xu, L.Y. Shi, T. Nonferr, Met. Soc. China 19 (2009) 1526–1532.
[15] C. Leach, N.K. Ali, D. Cupertino, R. Freer, Mater. Sci. Eng. B170 (2010) 15–21.
[16] R. Subasri, M. Asha, K. Hembram, G.V.N. Rao, T.N. Rao, Mater. Chem. Phys. 115 (2009) 677–684.
[17] M.L. Dinesha, H.S. Jayanna, S. Ashoka, G.T. Chandrappa, J. Alloys Compd. 485 (2009) 538–541.
[18] L. Saint Macary, M.L. Kahn, C. Estournes, P. Fau, D. Tremouilles, M. Bafleur, P. Renaud, B. Chaudret, Adv. Funct. Mater. 19 (2009) 1775–1783.
[19] C.W. Nahm, Mater. Sci. Eng. B170 (2010) 123–128.
[20] T.Y. Li, H.Q. Wang, Z.Q. Hua, L. Dong, H.W. Zhao, Y. Wang, Ceram. Int. 36 (2010) 1511–1516.
[21] J.A. Park, Physica B 403 (2008) 639–643.
[22] C.W. Nahm, Mater. Lett. 62 (2008) 4440–4442.
[23] C.W. Nahm, J. Alloys Compd. 490 (2010) L52–L54.

[24] C.W. Nahm, Ceram. Int. 36 (2010) 1109–1115.
[25] Z.Y. Lu, Y.Y. Cai, Z.W. Chen, J.Q. Wu, Rare Metal Mater. Eng. 36 (2007) 187–190.
[26] X.L. Song, F.Y. Liu, J. Chinese Ceram. Soc. 21 (1993) 345–348.
[27] Z.J. Peng, C.B. Wang, L.J. Gauckler, H.Z. Miao, Key Eng. Mater. 368–372 (2008) 479–482.
[28] X.L. Fu, W.H. Tang, Z.J. Peng, Acta Phys. Sinica 57 (2008) 5844–5852.
[29] A.A. Dakhel, J. Alloys Compd. 488 (2009) 31–34.
[30] I.C. Ostroski, M.A.S.D. Barros, E.A. Silva, J.H. Dantas, P.A. Arroyo, O.C.M. Lima, J. Hazard. Mater. 161 (2009) 1404–1412.
[31] M.S. Sahasrabudhe, S.I. Patil, S.K. Date, K.P. Adhi, S.D. Kulkami, P.A. Joy, R.N. Bathe, Solid State Commun. 137 (2006) 595–600.
[32] S.T. Li, F.Y. Liu, X.L. Song, J. Ceram. 18 (1997) 73–77.
[33] J.S. Kim, C.I. Cheon, P.W. Jang, Y.N. Choi, C.H. Lee, J. Eur. Ceram. Soc. 24 (2004) 1551–1555.
[34] J.S. Kim, C.I. Cheon, H.J. Kang, P.W. Jang, J. Eur. Ceram. Soc. 27 (2007) 3951–3954.
[35] J.F. Wang, W.B. Su, H.C. Chen, W.X. Wang, G.Z. Zang, J. Am. Ceram. Soc. 88 (2005) 331–334.
[36] K. Mukae, Am. Ceram. Soc. Bull. 66 (1987) 1329–1331.
[37] S. Bernik, N. Daneu, J. Eur. Ceram. Soc. 27 (2007) 3161–3170.
[38] K. Mukae, L. Ysuda, L. Nagasawa, Jpn. J. Appl. Phys. 16 (1977) 1361–1368.
[39] C.W. Nahm, B.C. Shin, B.H. Min, Mater. Chem. Phys. 82 (2003) 157–164.